Available online at www.sciencedirect.com
SCIENCE DIRECT®
Journal of Magnetic Resonance 175 (2005) 300–308
JMR Journal of Magnetic Resonance
www.elsevier.com/locate/jmr

The internal magnetic field distribution, and single exponential magnetic resonance free induction decay, in rocks

Quan Chen [a], Andrew E. Marble [a,b], Bruce G. Colpitts [b], Bruce J. Balcom [a,*]

[a] *MRI Centre, Department of Physics, University of New Brunswick, Fredericton, NB, Canada E3B 5A3*
[b] *Department of Electrical and Computer Engineering, University of New Brunswick, Fredericton, NB, Canada E3B 5A3*

Received 19 January 2005; revised 9 April 2005
Available online 6 June 2005

Abstract

When fluid saturated porous media are subjected to an applied uniform magnetic field, an internal magnetic field, inside the pore space, is induced due to magnetic susceptibility differences between the pore-filling fluid and the solid matrix. The microscopic distribution of the internal magnetic field, and its gradients, was simulated based on the thin-section pore structure of a sedimentary rock. The simulation results were verified experimentally. We show that the 'decay due to diffusion in internal field' magnetic resonance technique may be applied to measure the pore size distribution in partially saturated porous media. For the first time, we have observed that the internal magnetic field and its gradients in porous rocks have a Lorentzian distribution, with an average gradient value of zero. The Lorentzian distribution of internal magnetic field arises from the large susceptibility contrast and an intrinsic disordered pore structure in these porous media. We confirm that the single exponential magnetic resonance free induction decay commonly observed in fluid saturated porous media arises from a Lorentzian internal field distribution. A linear relationship between the magnetic resonance linewidth, and the product of the susceptibility difference in the porous media and the applied magnetic field, is observed through simulation and experiment.
© 2005 Elsevier Inc. All rights reserved.

Keywords: Internal magnetic field; Internal magnetic field gradients; Lorentzian distribution; Porous media; Single exponential free induction decay; SPRITE MRI

1. Introduction

The microscopic heterogeneity of realistic porous media yields a heterogeneous distribution of magnetic fields in porous media examined with magnetic resonance. The distribution of local magnetic fields in the pore space would ordinarily be considered a challenge, or a problem, for magnetic resonance investigations. However, the distribution of the local magnetic fields has several general features which are highly advantageous for magnetic resonance (MR) experimentation. The current work examines the origin, and consequence of the field distribution for "decay due to diffusion in internal field' (DDIF) [1] and magnetic resonance imaging (MRI) investigations of porous media.

The heterogeneous character of the local magnetic field due to susceptibility contrast in porous media, biological tissues, and other inhomogeneous media is a very active research subject in MR, since it impacts a wide range of different MR measurements. Diffusion of nuclei through the inhomogeneous magnetic field results in additional transverse relaxation [2]. The internal magnetic gradient within these inhomogeneous media may interfere with experimentally applied gradients and lead to artifacts in MR diffusion and imaging measurements [3].

The magnetic field distribution in porous media, with an external static magnetic field applied, has been studied for many years. The magnetic fields from randomly

* Corresponding author. Fax: +1 506 4534581.
E-mail address: bjb@unb.ca (B.J. Balcom).

1090-7807/$ - see front matter © 2005 Elsevier Inc. All rights reserved.
doi:10.1016/j.jmr.2005.05.001

placed dipoles, an approximation of porous media behavior, were first studied by Brown [4] in 1961. Drain [5] calculated the NMR line broadening due to field inhomogeneities in powdered samples with a loosely packed sphere model, and a close packed sphere model. Sen and Axelrod [6] reviewed previous studies on internal magnetic fields, and investigated the internal field distribution in a cylinder pack. Their study showed, quite naturally, that internal field variations occur over the length scale of the pores. Audoly et al. [7] studied the internal field distribution in a dense random pack of spheres using numerical computation. Their calculations showed that the spatial correlation of the internal field decays over the length scale of the pores, and that the magnetic field correlation function is very similar to the structure factor of the porous media.

Inhomogeneously broadened linewidths, for fluid saturated porous media, are due to the observed nuclei having a range of resonance frequencies, i.e., a range of local magnetic fields. The NMR line shape and linewidth may be obtained by Fourier transformation of the simple free induction decay (FID) experiment.

The FID is observed to be single exponential for most sedimentary rocks [8] and concretes [9], and the effective spin–spin relaxation time (T_2^*) is largely insensitive to fluid saturation [8]. The reason for single exponential T_2^* decay in porous media is discussed in the current paper and is based also on studies of the internal magnetic field distribution in Berea sandstone. The single exponential T_2^* behavior [8], of fluid saturated porous media, is critical to the success of density weighted centric scan SPRITE MRI [10,11].

In recent work [8], we combined 'decay due to diffusion in internal field' (DDIF) [1] measurements with 3D Conical-SPRITE MRI [10,11] to study the dynamic processes of spontaneous co-current and counter-current imbibition. Dynamic flow processes were monitored by DDIF water filled pore size distribution measurements, while the in situ 3D water content was detected by 3D Conical-SPRITE MRI during spontaneous imbibition. Different pore- and throat-filling mechanisms were revealed for co-current imbibition and counter-current imbibition in natural porous media [8]. However, the DDIF measurement of partially saturated Berea sandstone was based on a critical assumption that the internal field distribution in the water phase resembled that of a fully saturated sample. This assumption was reasonable since the susceptibility difference between the Berea sandstone and air was similar to the difference between Berea sandstone and water.

The validity of DDIF, for partially saturated porous media, requires that the internal field distribution of a fully saturated porous medium be similar to that in the partially saturated sample. Based on the pore structure of a thin section of Berea sandstone, the microscopic distributions of the internal magnetic fields in a fully (water) and partially saturated (water and air) Berea sandstone were simulated as part of the current paper.

2. Calculation of the internal magnetic field and its gradients

The internal magnetic induction **B** induced by applied field $\mathbf{H}_0$ is the solution of a set of two static equations:

$$\nabla \bullet \vec{B} = 0, \tag{1}$$

$$\nabla \times \vec{H} = 0, \tag{2}$$

with the constitutive relationship between magnetic flux density **B** and magnetic field intensity **H**

$$\vec{B} = \mu_0(1 + \chi(x,y))\vec{H}, \tag{3}$$

where $\mu_0 = 4\pi \times 10^{-7}$ H/m is the permeability of vacuum. The magnetic susceptibility χ will have a spatial dependence according to the pore structure of a porous media sample.

The effects of susceptibility inhomogeneities on the magnetic field applied to a realistic, model porous media sample were studied numerically. Fig. 1 shows a thin-section optical image of a Berea sandstone sample. The large white regions are quartz crystals while the

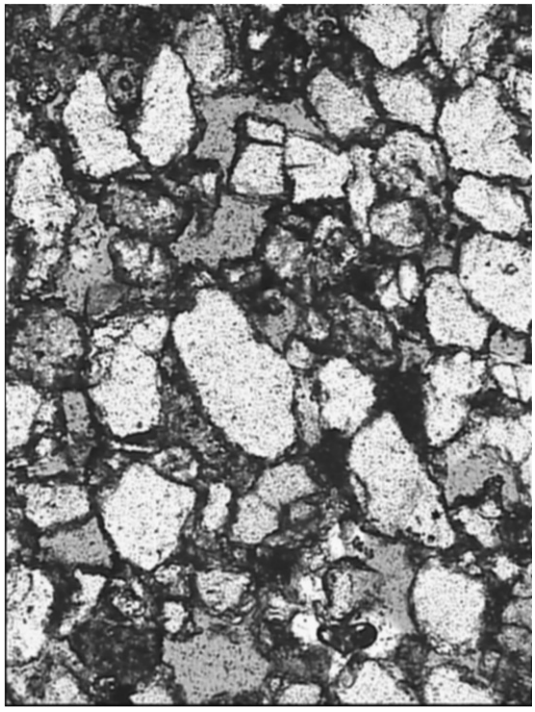

Fig. 1. An optical micrograph of a Berea sandstone thin-section, with a field of view (FOV) of 921 μm × 1228 μm. The white regions are large quartz crystals, while dark regions are small crystals and clay. The gray regions are pore space identified by the dye color of an impregnated resin.

darker regions are small crystals and clay. The gray regions represent the pore space, as determined by saturating the sample with a colored resin. For simulation purposes, the pore shapes from several thin-section images were optically scanned and then segmented with a binary mask. These pore shapes were assembled in a software model to give a simulated cross-section with a porosity of 18.6%. Fig. 2 shows the simulation model used. In this cross-section, the water saturation of the pore space is 100%. The lighter regions represent the water filled pores. When the porous media are only partially saturated, the water may occupy the pores fully or partially. The partially saturated pores are always more water-wet than air-wet. The water spreads on the surface of the pore space, while the air occupies the pore center [12]. To simulate this effect, air voids of varying sizes were added to the simulation model to achieve a water saturation of 60%. Fig. 3 shows the simulation model with the air voids represented by the circular voids within the pores.

A commercial finite element simulation package, FEMLAB (Comsol, Burlington, MA), was employed to calculate the internal field distribution by solving Eqs. (1)–(3) numerically. The geometries shown in Figs. 2 and 3 were simulated with an uniform field (B_0) of 2.4 T in the horizontal (z) direction. We assume that each phase within the sample has a homogeneous and isotropic susceptibility. The susceptibility values (SI units) for the matrix, water, and air were: $\chi[\text{Berea}] = 89.85 \times 10^{-6}$, $\chi[\text{water}] = -9.05 \times 10^{-6}$, and $\chi[\text{air}] = 0.36 \times 10^{-6}$. Hürlimann [2] showed that the susceptibility value of Berea is typical in sandstones.

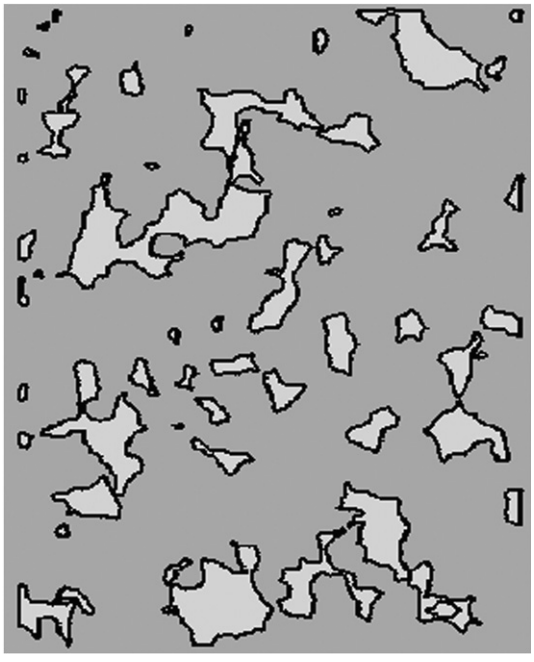

Fig. 2. A 2D simulation model for a 100% water saturated Berea sandstone, which was extracted from the thin-section images. FOV, 921 μm × 1228 μm. Gray and white represent solid matrix and water, respectively.

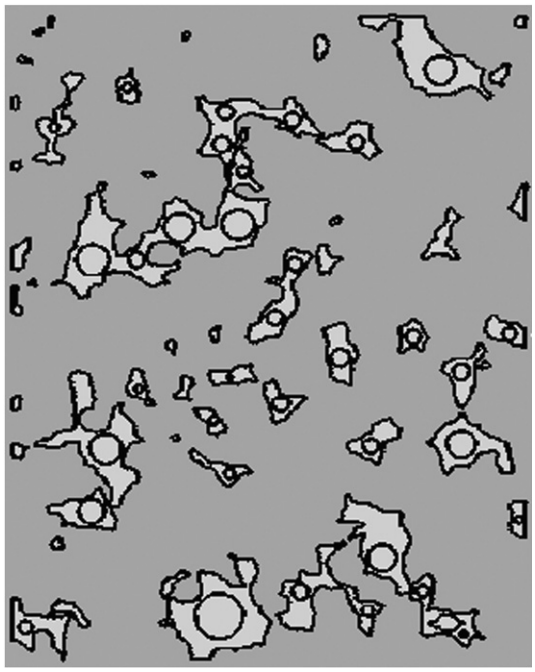

Fig. 3. A 2D simulation model for a Berea sandstone saturated with water and air, where the water spreads on the surface of the pore space, while the air occupies the pore center, due to the effect of wettability. FOV, 921 μm × 1228 μm. Gray and white represent solid matrix and water, respectively. The circles represent air bubbles.

It should be emphasized that we always refer to the internal field and its gradients in the water phase, since this is where the magnetic resonance signal originates, and further we focus on the z-components of the internal field and its gradients, because they are more relevant to MR, in particular, the DDIF measurement. The two-dimensional internal field (B_z^i) distributions in the water phase, for Berea sandstone saturated with water, and the water/air bearing sample are shown in Figs. 4 and 5, respectively. A histogram plot of the internal field (B_z^i) distribution, scaled to the dimensionless form, $(B_z^i - B_0)/(\Delta\chi B_0)$, in the water phase for a fully water saturated Berea sandstone is shown in Fig. 6.

A Lorentzian lineshape is fit to the distributions as illustrated in Fig. 6. Its linewidth (full width at half maximum, FWHM) was 0.3 in dimensionless form. A histogram plot of the internal field (B_z^i) distribution (scaled as in Fig. 6) in the water phase for a water/air saturated sample is reproduced in Fig. 7, a Lorentzian fit is also shown in this Figure. The FWHM linewidth is 0.32 in dimensionless form. The amplitudes of all histogram plots in the paper are scaled to the water saturation values. The overall lineshapes of fully and partially water saturated Berea samples, in Figs. 6 and 7 are similar to the Lorentzian distribution, except for small scale

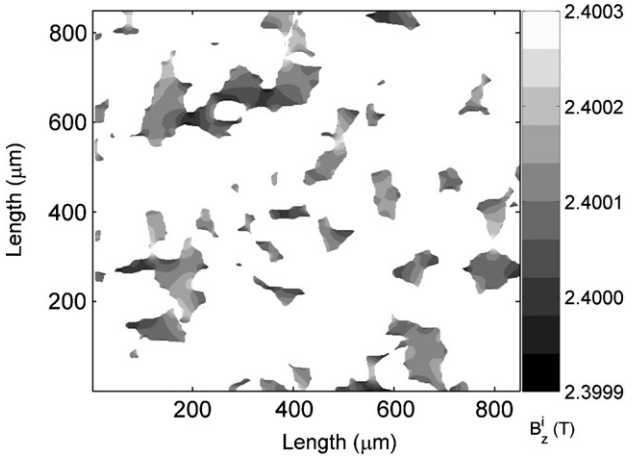

Fig. 4. Internal magnetic field (B_z^i) distribution in the water phase for Berea saturated with water, determined through simulation. FOV, 850 μm × 850 μm and spatial resolution, 1.1 μm. The external field ($B_0 = 2.4$ T) is applied in the horizontal (z) direction, from left to right. The grayscale bar on the righthand side of the figure indicates the magnitude of the internal field.

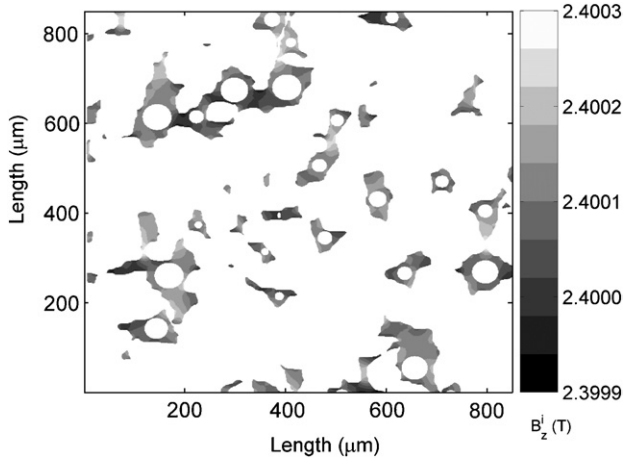

Fig. 5. Internal magnetic field (B_z^i) distribution in the water phase for Berea saturated with water and air, determined through simulation. FOV, 850 μm × 850 μm and spatial resolution, 1.1 μm. The external field ($B_0 = 2.4$ T) is applied in the horizontal (z) direction, from left to right. The grayscale bar on the righthand side of the figure indicates the magnitude of the internal field.

structure which we believe is due to the restricted field of view (FOV) 850 by 850 μm, employed in the simulation.

The simulations show that the internal field is proportional to the external magnetic field (B_0), and the susceptibility difference ($\Delta\chi$), and is bounded with a maximum and a minimum field. The internal field within a pore is inhomogeneous with a spatial variation primarily over the length scale of the pore size. Rapid field oscillation within individual pores is not observed. These results are similar to the internal field distribution in a Finney pack calculated by Audoly et al. [7]. The overall lineshapes obtained by simulation were approximately Lorentzian, with a small scale structure outlined above.

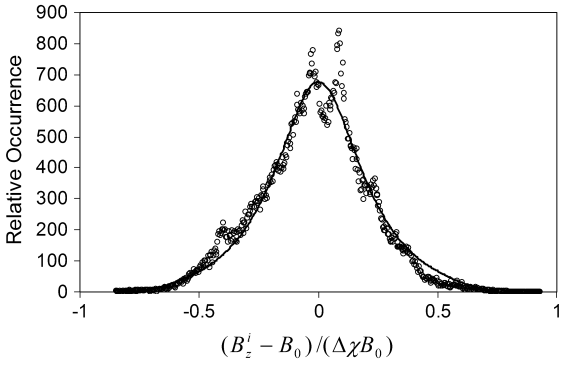

Fig. 6. Histogram plot of the internal magnetic field ($B_z^i, \circ$) distribution (scaled with dimensionless form: $(B_z^i - B_0)/\Delta\chi B_0$) in the water phase for a fully water saturated Berea sandstone, determined through simulation, with a linewidth (FWHM) of 0.3. The best fit line is a Lorentzian function, with R^2 of 0.97.

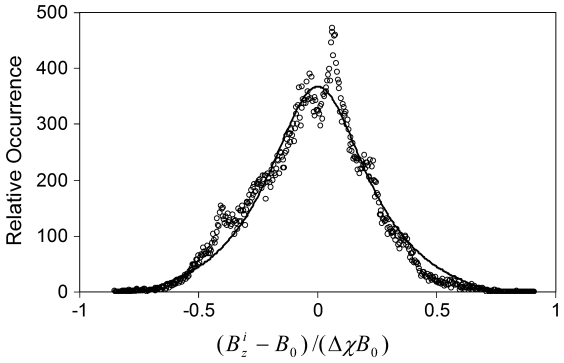

Fig. 7. Histogram plot of the internal magnetic field ($B_z^i, \circ$) distribution (scaled with dimensionless form: $(B_z^i - B_0)/\Delta\chi B_0$) in the water phase for a Berea sandstone saturated with water and air, determined through simulation, with a linewidth (FWHM) of 0.32. The best fit line is a Lorentzian function, with R^2 of 0.96. Note that the reduced overall area is due to less water present. The distribution width and overall shape has not changed significantly, although the fine structure is reduced.

These effects are averaged out in a bulk FID measurement of a larger sample due to an intrinsic disordered pore structure in porous media, which results in an 'effective' Lorentzian field distribution and a single exponential FID decay. The Lorentzian lineshape of the MR absorption spectrum for a water saturated Berea sandstone is shown in Fig. 8, which was obtained by Fourier transform of the bulk FID measurement data with a static field (B_0) of 2.4 T. This experimental result verifies the Lorentzian internal field distribution determined by our simulation. Because the lineshape of the MR absorption spectrum is directly related to the magnetic field distribution, for these short T_2^* samples, diffusion can be ignored.

A comparison of histogram plots for the internal field distribution between a fully and partially water saturated pore is reported in Fig. 9. The two cases

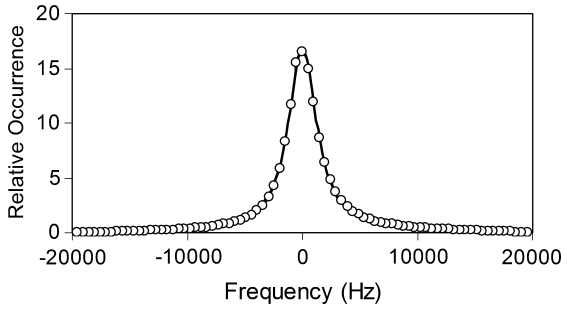

Fig. 8. MR absorption lineshape for a water saturated Berea sandstone obtained by FID measurement (○) with a static magnetic field (B_0) of 2.4 T. The best fit line is a Lorentzian function, with R^2 of 0.999.

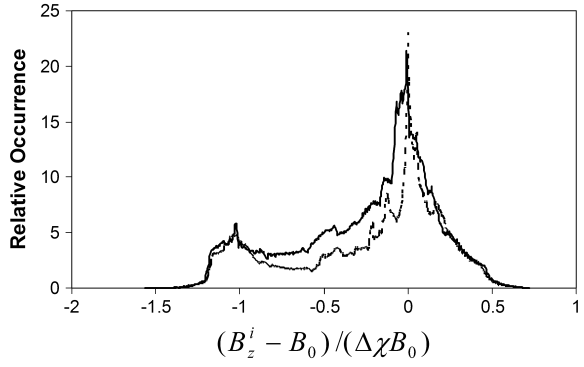

Fig. 9. A comparison of histogram plots of the internal magnetic field (B_z^i) distribution in the water phase within a fully (—) and partially (---) water saturated single pore, determined through simulation, B_0 of 2.4 T.

have very similar internal field distributions; the areas under the histogram plots are scaled with the water saturation values. Note that deviation of the lineshape from a pure Lorentzian is significant due to the very small FOV of 120 by 120 μm, where there is just one pore.

The internal field distribution for a fully saturated Berea sandstone is similar to the partially water saturated sample. This is also true for individual pores.

Plots of the simulated two-dimensional internal gradient (G_z^i) distributions in the water phase, for Berea saturated with water and with water/air, are shown in Figs. 10 and 11, respectively. The plot's range of gradient values is restricted between ±10 T/m for purposes of display, since most gradient values are in the selected range, which is indicated in Figs. 12 and 13. A histogram plot of the simulated internal gradient (G_z^i) distribution in the water phase, for Berea saturated with water, and the sample partially saturated with water, are shown in Figs. 12 and 13. The amplitudes of the histogram plots are scaled with the water saturation values. Their FWHMs are 3.5 and 4.2 T/m, respectively. The maximum gradient is more than 80 T/m. These magnetic field

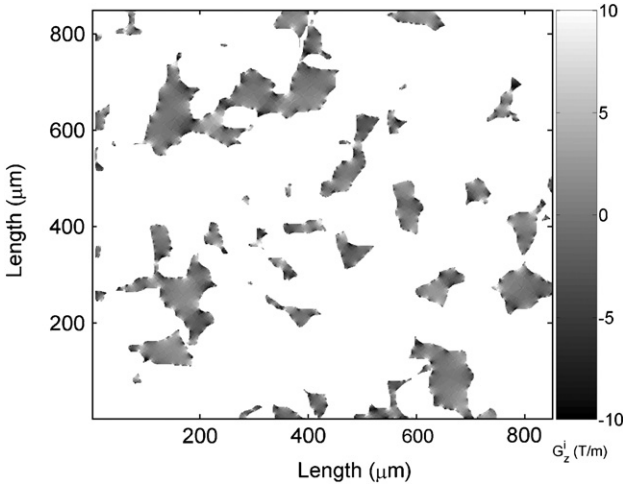

Fig. 10. Internal magnetic field gradient (G_z^i) distribution in the water phase for a Berea sample saturated with water, determined through simulation. FOV, 850 μm × 850 μm and spatial resolution, 1.1 μm. The external field ($B_0 = 2.4$ T) is applied in the horizontal (z) direction, from left to right. The plot's range of gradient values is restricted to ±10 T/m for purposes of display. The grayscale bar on the righthand side of the figure indicates the magnitude of the internal gradient.

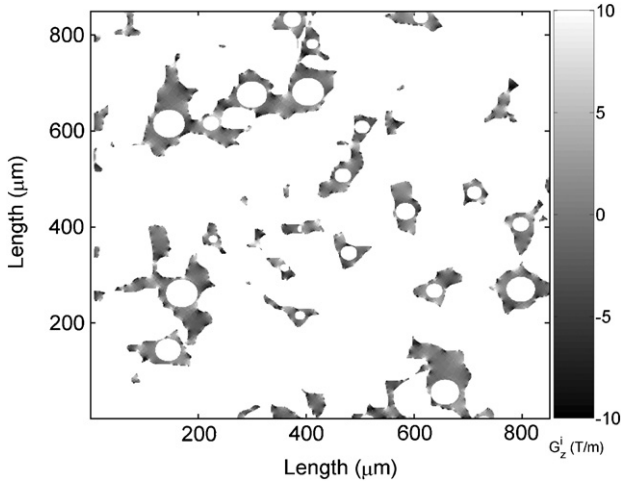

Fig. 11. Internal magnetic field gradient (G_z^i) distribution in water phase for Berea saturated with water and air, determined through simulation. FOV, 850 μm × 850 μm and spatial resolution, 1.1 μm. The external field ($B_0 = 2.4$ T) is applied in the horizontal (z) direction, from left to right. The plot's range of gradient values is restricted to ±10 T/m for purposes of display. The grayscale bar on the righthand side of the figure indicates the magnitude of the internal gradient.

gradients are very strong compared with the external gradients applied for MRI and diffusion measurement. The simulation results indicate that the internal gradient changes rapidly within a pore, and is usually stronger near the surface of the pore than in the center of the pore. The histogram plots of the internal gradient distributions are smooth and symmetrical, without sharp features, with an average gradient of zero. The fit result shows that the internal gradient distribution has a near

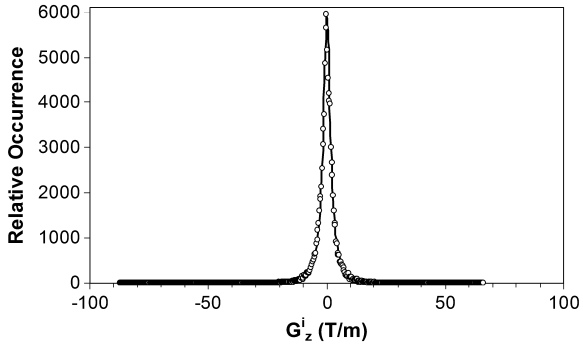

Fig. 12. Histogram plot of the internal magnetic field gradient (G_z^i, ○) distribution in the water phase for a water saturated Berea sample, determined through simulation, with a linewidth of 3.5 T/m, B_0 of 2.4 T. The best fit line is a Lorentzian function with zero-mean and R^2 of 0.992.

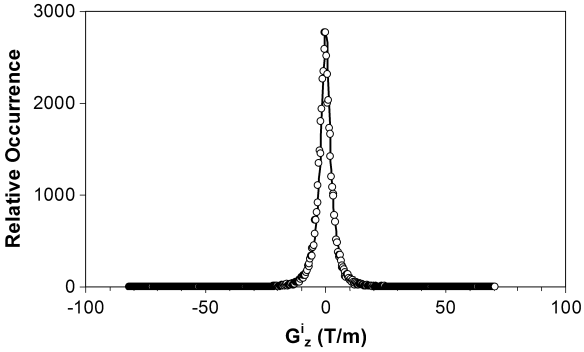

Fig. 13. Histogram plot of the internal magnetic field gradient (G_z^i, ○) distribution in the water phase for a Berea sample saturated with water and air, determined through simulation, with a linewidth of 4.2 T/m, B_0 of 2.4 T. The best fit line is a Lorentzian function with zero-mean and R^2 of 0.996.

perfect Lorentzian lineshape. Note that the internal gradients scale in a manner similar to the linewidth, $\Delta\chi B_0$. We show only the result for a 2.4 T external field (B_0) in Figs. 12 and 13.

A comparison of histogram plots for the internal gradient distribution between a fully and partially water saturated pore is reported in Fig. 14, which indicates a similar distribution for both cases. The areas under the histogram plots are scaled with the water saturation values. The internal magnetic field gradient distributions in each individual pore span both positive and negative values.

As with the internal magnetic field, the gradient distribution for a fully saturated Berea sandstone is similar to that of the partially water saturated Berea sandstone. These results indicate that DDIF may be employed to explore the water filled pore size distribution for partially saturated Berea sandstone. Our previous assumption [8], based on similar susceptibility differences for rock/water and rock/air is therefore verified.

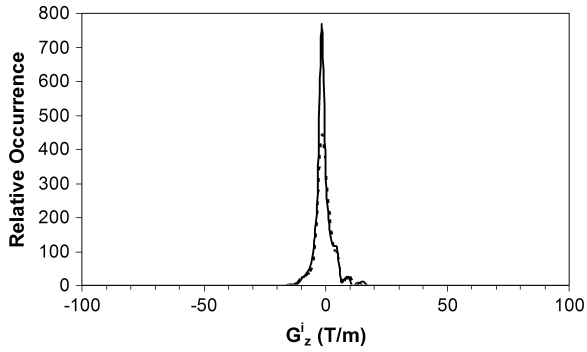

Fig. 14. A comparison of histogram plots of the internal magnetic field gradient (G_z^i) distribution in the water phase within a fully (—) and partially (---) water saturated single pore, determined through simulation, B_0 of 2.4 T.

3. Implications of a distribution of the internal magnetic field and its gradients

Our simulation results demonstrated that the internal magnetic field gradients in porous media, even within each individual pore, are rapidly varying spatially, and have a broad distribution of both polarities. They should not be considered in term of a single fixed gradient value experienced by spins in the sample. The spatial characteristics of the internal field are important for many NMR experiments.

Many studies have analyzed the statistical distribution of internal gradients (**G**) with spin-echo or CPMG sequences. For example, Hürlimann [2] reported the major features of diffusion in internal gradients with the concept of an effective gradient and an estimation of the distribution of the internal gradients. He also pointed out that there are three length scales which effect attenuation of the Hahn echo amplitude in heterogeneous fields. Sun and Dunn [13] devised a modified CPMG sequence to produce a two-dimensional plot of apparent internal field gradient distribution as a function of T_2 relaxation time.

The distribution of the internal gradients determined by our simulation results is obviously independent of molecular diffusion effect. However, the internal gradients obtained with CPMG measurements [2,13] are averaged over a specified distance through which the spins are able to diffuse. Therefore, when the diffusion distance is changed, the measured effective gradient distribution may also change. In addition, CPMG analysis is based on $\mathbf{G}^2$ rather than **G**, and there may be a restricted diffusion effect.

Many efforts have been made to suppress artifacts from internal magnetic field gradients in pulse field gradient diffusion measurements. Karlicek and Lowe [14] designed an alternating pulse field gradient combined with a spin-echo measurement. Cotts et al. [15] developed several sequences based on bipolar gra-

dients and stimulated echoes (STE) for samples with short spin–spin relaxation time. Latour et al. [16] proposed a sequence combining a series of alternating pulse field gradients with STE-CPMG. However, the basic assumption for the successful cancellation of the cross-term between the internal gradient and an externally applied gradient is that the each diffusing spin experiences a constant internal gradient in the encoding and decoding intervals of the pulse sequence. Sun et al. [17] and Galvosas et al. [18] introduced an asymmetric field gradient ratio diffusion encoding sequence to suppress the cross-term between the applied gradient and internal gradient during the encoding and decoding intervals, independently. This method still requires that the internal gradients experienced by each individual spin are constant over the encoding and decoding intervals. Our simulation results show that the internal gradients in porous rocks, even in individual pores, have a rapid spatial variation and a broad distribution of both signs. This means that all current methods for diffusion measurement in porous media are unable to completely cancel artifacts due to the internal magnetic field in these samples.

The Lorentzian distribution of the internal magnetic field gradient, suggested by the current simulations, should prove very useful for the analysis of transverse relaxation and diffusion effects in porous media.

4. Single exponential T_2^* decay in porous media

The effective spin–spin relaxation time (T_2^*) may be analyzed through a free induction decay (FID) measurement. The overall FID decay rate ($1/T_2^*$), Eq. (4), may be represented as the sum of contributions due to the spin–spin relaxation rate ($1/T_2$), the underlying B_0 inhomogeneity ($1/T_{2m}$), in addition to an internal field (B^i) induced by the susceptibility difference ($\Delta\chi$) between the pore fluid and solid matrix ($1/T_{2i}$). The $1/T_{2m}$ term is usually insignificant

$$1/T_2^* = 1/T_2 + 1/T_{2m} + 1/T_{2i}. \tag{4}$$

In most sedimentary rocks and concretes, there is a large susceptibility difference between the pore-filling fluid and solid matrix due to paramagnetic impurities in the solid matrix. The average pore size is on the order of 10–100 μm and T_2^* is on the order of 10–100 μs. A wide range of experimental results [8] show that the overall FID decay rate ($1/T_2^*$) is dominated by the $1/T_{2i}$ term, and the first and second terms on the right side of Eq. (4) can be neglected. This is confirmed by the strong internal gradients observed in our simulation results and yields an 'effective' single exponential T_2^* decay. This single exponential T_2^* decay is observed even for rocks partially water saturated.

The decay rate of the FID and the corresponding NMR linewidth ($\Delta\nu = 1/\pi T_2^*$) for water in porous rocks may be estimated by [19]

$$\frac{1}{\pi T_{2i}} = \frac{\gamma \Delta B^i}{2\pi}, \tag{5}$$

where ΔB^i is the width of magnetic field distribution due to susceptibility contrast in fluid saturated rocks. Our internal field simulation in the previous section shows that ΔB^i is proportional to the susceptibility difference between the water and rock matrix, and to the strength of the applied magnetic field. Thus,

$$\Delta B^i = C\Delta\chi B_0, \tag{6}$$

where C is a dimensionless constant.

Combining Eqs. (5) and (6), as well as the Larmor equation, yields an expression for $\Delta\nu$, the frequency range

$$\Delta\nu \approx \frac{1}{\pi T_{2i}} = \frac{\gamma \Delta B^i}{2\pi} = C\Delta\chi f_0, \tag{7}$$

where $f_0 = \frac{\gamma B_0}{2\pi}$ is the Larmor frequency, γ is the gyromagnetic ratio, while C is a dimensionless constant.

Fig. 15 shows an experimental single exponential, T_2^* decay in a fully water saturated Berea sandstone following an RF pulse. The data was fit to the equation

$$S(t) = M_0 e^{-t/T_2^*} \sin\theta, \tag{8}$$

where S is the NMR signal intensity and M_0 is the equilibrium sample magnetization, while the angle θ is the RF pulse flip angle. The variable t is the time following the RF pulse. The fit T_2^* was 127 μs. Experimental results [8] show that the T_2^* of the Berea sandstone samples varied from 114 to 127 μs when the water saturation was varied from 9.1 to 100%, but remained single exponential, despite multi-exponential T_2 behavior. This multi-exponential character is well known to be correlated with the pore size distribution in the rock [20].

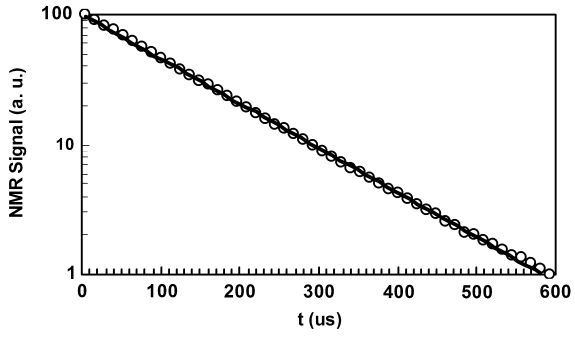

Fig. 15. A FID decay measurement for a water saturated Berea sandstone at a static magnetic field (B_0) of 2.4 T. The single exponential best fit line has a decay time constant T_2^* of 127 μs. The single exponential T_2^* decay behavior is very general for sedimentary rocks and concretes, with different fluid saturations, at different magnetic field strengths.

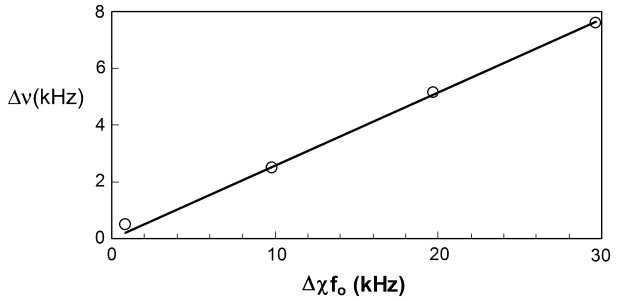

Fig. 16. NMR linewidth measured at four different magnetic fields (B_0) (7.0, 4.7, 2.4, and 0.2 T) for a water saturated Berea sandstone. There is a linear relationship between the linewidth ($\Delta\nu$) and the product of the susceptibility difference ($\Delta\chi$) and Larmor frequency (f_0). The best fit line is given by $\Delta\nu = 0.26\Delta\chi f_0$.

The experimental NMR linewidths of the Berea sandstone sample at four different magnetic field strengths (7.0, 4.7, 2.4, and 0.2 T) are reported in Fig. 16. Note a linear relationship between the linewidth and the product of the susceptibility difference and the Larmor frequency is predicted by Eq. (7). This result was predicted by the simulations of Fig. 6 and confirmed experimentally in Fig. 16. The value of the proportionality C, 0.26 in Eq. (7), is obtained by experiment. The simulated result, Fig. 6, has a C value of 0.3 in Eq. (7). This calculated result is remarkably similar to the FID measurement result. These results indicate that our 2D model is a reasonable approximation to real 3D samples for simulation of the statistical properties of the internal magnetic field in porous materials. We have observed single exponential FID decay in a wide range of sedimentary rocks [8] and concretes [9], with T_2^* largely insensitive to water saturation change [8]. This powerful yet simple feature permits facile spin density imaging for centric scan SPRITE MRI, [8,10,11], since the local image intensity, also expressed by Eq. (8), features relaxation decay which is purely T_2^* in nature [21].

5. Conclusions

Our results show that the internal magnetic field is proportional to the external magnetic field (B_0) and the susceptibility difference ($\Delta\chi$), and is bounded with a maximum and a minimum field. The internal field within a pore is inhomogeneous and its spatial variation occurs primarily over the length scale of the pore size. The internal magnetic field gradients in porous rocks are very strong compared to the external gradients applied for MRI and diffusion measurement. For the first time, we have shown that the internal gradients in porous rocks have a Lorentzian distribution, with an average gradient value of zero. This zero-mean Lorentzian distribution will be very useful for analyzing transverse relaxation and diffusion measurements in porous media.

The internal magnetic field, and magnetic field gradient distribution, for a fully saturated Berea sandstone are similar to those for a partially saturated sample. These results indicate that DDIF may be employed to explore the water filled pore size distribution for a partially saturated medium.

The overall field distribution and MR linewidth for a water saturated Berea sandstone, calculated by numerical simulation, are consistent with the bulk experimental FID measurement results at different magnetic field strengths.

A single exponential FID decay is observed in most sedimentary rocks and concretes, and the effective spin–spin relaxation times (T_2^*) are largely insensitive to water saturation in these samples. The single exponential T_2^* behavior arises from an 'effective' Lorentzian distribution of the internal field, induced by the large susceptibility contrast and an intrinsic disordered pore structure in these porous media. These features ensure that centric scan SPRITE is a natural spin density imaging method, since its local image intensity has simple T_2^* contrast.

6. Experimental

Berea sandstone samples were employed for all the experiments. Its porosity (the ratio of pore volume to bulk volume of rock) was 18.6% and permeability 0.18 μm^2. All samples were dried at 80 °C until constant mass was achieved. The samples were fully saturated with distilled water under vacuum conditions. The rock sample was sealed with Teflon seal tape to avoid evaporation during NMR measurements.

NMR experiments were performed in four different magnets. A 2.4 T 16 cm i.d. horizontal bore superconducting magnet (Nalorac Cryogenics, Martinez, CA), with a proton-free 4.7 cm i.d. eight-rung quadrature birdcage RF probe (Morris Instruments, Ottawa, ON), driven by a 2 kW 3445 RF amplifier (American Microwave Technology, Brea, CA), and a 4.7 T of 8 cm i.d. vertical bore superconducting magnet (Nalorac Cryogenics, Martinez, CA), with a Litz RF volume coil DSI-874 (Doty Scientific, Columbia, SC) with 2.2 cm i.d., driven by a 300 W RF amplifier (American Microwave Technology, Brea, CA), and a 0.2 T permanent magnet with a 12 cm pole gap, with a homemade single turn solenoid coil with 3 cm i.d., driven by a 300 W M3205A RF amplifier (American Microwave Technology, Brea, CA) were employed. All three magnets were controlled with Apollo consoles (Tecmag, Houston, TX). A 7 T 16 cm i.d. horizontal bore superconductive magnet (Magnex Scientific, Oxford, UK), with a 6.2 cm i.d. home made birdcage RF probe, driven by a 400 W RF 8T400 amplifier (Communication Power, Brentwood, NY) was utilized, the console was a MARAN-DRX (Resonance Instruments, Witney, UK).

Acknowledgments

B.J.B. thanks NSERC of Canada for operating and equipment grants. B.J.B. also thanks the Canada Chairs program for a Research Chair in MRI of Materials (2002–2009). The UNB MRI Centre is supported by an NSERC Major Facilities Access Grant. B.J.B. and Q.C. thank the Atlantic Innovation Fund for project support. We also thank R.P. MacGregor for his technical assistance.

References

[1] Y.-Q. Song, S. Ryu, P.N. Sen, Determine multiple length scales in rocks, Nature (London) 406 (2000) 178–181.
[2] M.D. Hürlimann, Effective gradients in porous media due to susceptibility differences, J. Magn. Reson. 131 (1998) 232–240.
[3] P.T. Callaghan, Principles of Nuclear Magnetic Resonance Microscopy, Oxford University Press, New York, 1993.
[4] R.J.S. Brown, Distribution of fields from randomly placed dipoles: free-precession signal decay as a result of magnetic grains, Phys. Rev. 121 (1961) 1379–1382.
[5] L.E. Drain, The broadening of magnetic resonance lines due to field inhomogeneity in powdered samples, Phys. Soc. Proc. 80 (1962) 1380–1382.
[6] P.N. Sen, S. Axelrod, Inhomogeneity in local magnetic field due to susceptibility contrast, J. Appl. Phys. 86 (1999) 4548–4554.
[7] B. Audoly, P.N. Sen, S. Ryu, Y.-Q. Song, Correlation function for inhomogeneous magnetic field in random media with application to a dense random pack of spheres, J. Magn. Reson. 164 (2003) 154–159.
[8] Q. Chen, M. Gingras, B.J. Balcom, A magnetic resonance study of pore filling processes during spontaneous imbibition in Berea sandstone, J. Chem. Phys. 119 (2003) 9609–9616.
[9] S.D. Beyea, Magnetic Resonance Imaging (MRI) and Relaxation Time Mapping of Concrete, PhD. Thesis, University of New Brunswick, 2000.
[10] B.J. Balcom, R.P. MacGregor, S.D. Beyea, D.P. Green, R.L. Armstrong, T.W. Bremner, Single-point ramped imaging with T_1 enhancement (SPRITE), J. Magn. Reson. A 123 (1996) 131–134.
[11] M. Halse, D.J. Goodyear, B. MacMillan, P. Szomolanyi, D. Matheson, B.J. Balcom, Centric scan SPRITE magnetic resonance imaging, J. Magn. Reson. 165 (2003) 219–229.
[12] F.A.L. Dullien, Porous Media: Fluid Transport and Pore Structure, second ed., Academic Press, New York, 1991.
[13] B. Sun, K.-J. Dunn, Probing the internal field gradients of porous media, Phy. Rev. E 65 (2002) 51309.
[14] M.F. Karlicek Jr., I.J. Lowe, A modified pulsed gradient technique for measuring diffusion in the presence of large background gradients, J. Magn. Reson. 37 (1980) 75–91.
[15] R.M. Cotts, M.J.R. Hoch, T. Sun, J.T. Markert, Pulsed field gradient stimulated echo methods for improved NMR diffusion measurements in heterogeneous systems, J. Magn. Reson. 83 (1989) 252–266.
[16] L.L. Latour, L. Lin, C.H. Sotak, Improved PFG stimulated-echo method for the measurement of diffusion in inhomogeneous fields, J. Magn. Reson. B 101 (1993) 72–77.
[17] P.Z. Sun, J.G. Seland, D. Cory, Background gradient suppression in pulsed gradient stimulated echo measurements, J. Magn. Reson. 161 (2003) 168–173.
[18] P. Galvosas, F. Stallmach, J. Kärger, Background gradient suppression in stimulated echo NMR diffusion studies using magic pulsed field gradient ratios, J. Magn. Reson. 166 (2004) 164–173.
[19] J. Kärger, H. Pfeifer, S. Rudtsch, The influence of internal magnetic field gradients on NMR self-diffusion measurements of molecules adsorbed on microporous crystallites, J. Magn. Reson. 85 (1989) 381–387.
[20] R.L. Kleinberg, W.E. Kenyon, P.P. Mitra, Mechnism of NMR relaxation of fluids in rock, J. Magn. Reson. 108 (1994) 206–214.
[21] Q. Chen, M. Halse, B.J. Balcom, Centric scan SPRITE for spin density imaging of short relaxation time porous materials, Magn. Reson. Imaging 23 (2005) 263–266.